Journal of Alloys and Compounds 828 (2020) 154287

Contents lists available at ScienceDirect

Journal of Alloys and Compounds

journal homepage: http://www.elsevier.com/locate/jalcom

Topological analysis of electron density in half-Heusler ZrXBi (X = Co, Rh) compounds: A density functional theory study accompanied by Bader's quantum theory of atoms in molecules

M. Yazdani-Kachoei , S. Jalali-Asadabadi *

Department of Physics, University of Isfahan (UI), Hezar Gerib Avenue, Isfahan, 81746-73441, Iran

ARTICLE INFO

Article history:
Received 1 October 2019
Received in revised form
7 February 2020
Accepted 10 February 2020
Available online 12 February 2020

Keywords:
Zr-based compounds
Density functional theory
Charge density
Topological analysis
Quantum theory of atoms in molecules
Bader

ABSTRACT

Here, we study the electron charge densities (ECDs) of two half-Heusler compounds, i.e. ZrCoBi and ZrRhBi, from topological point of view using the combination of DFT and quantum theory of atoms in molecules (DFT + QTAIM). We also investigate the structural properties and electronic structures of these compounds including DOSs, band structures and electron charge densities (ECDs) as well as the thermoelectric parameters including Seebeck coefficient and electrical conductivity. Furthermore, the effects of pressure on the properties of these compounds are investigated. The DFT + QTAIM calculations show that the compounds under study have similar numbers and types of critical points, but different bonds properties. The bonds of the Rh-case are more stable than those of the Co-case. Moreover, the ECD values at bonds of Rh-case are more than the Co-case. Imposing pressure affects some properties of the bonds in both cases, but does not change the numbers and types of their critical points. Based on our electronic structure calculations, Co-case has sharper valence DOSs near the Fermi level and larger band gap compared to the Rh-case. We have also observed flatter bands in the Co-case near the Fermi level compared to the Rh-case. In the anticipation of further study, the presented results may provide fundamental information which can pave the way for the study on the thermoelectric efficiencies of these interesting thermoelectric materials. In agreement with the electronic structure, our thermoelectric calculations show higher Seebeck coefficient and lower electrical conductivity for ZrCoBi than ZrRhBi.

1. Introduction

Understanding the electronic structures and bonding properties of thermoelectric materials is crucial for improving their efficiencies [1–4]. Based on the kinetic theory, the lattice part of thermal conductivity which is a key parameter in thermoelectricity is drastically related to the chemical composition and bonding [1,2]. Moreover, the electrical and electronic parts of thermal conductivities of materials strongly depend on their band structures and densities of states (DOSs) [3,4]. Sharper DOS near the Fermi level can lead to a higher Seebeck coefficient [3,4]. Lower band gap in semiconductors can lead to a higher electrical conductivity [3].

All the above evidences show that electronic structures and bonding properties can play an important role for interpreting thermoelectric behaviors of materials. According to our recent study [5], a combination of density functional theory (DFT) [6,7] and Bader's quantum theory of atoms in molecules (QTAIM) [8–11], i.e. DFT + QTAIM, can provide a reliable *ab initio* approach to quantitatively shed light on the electronic structures and bonding properties of materials [5,12–15]. QTAIM is based on the topological analysis of electron charge density (ECD) [8–11] and the ECD can be calculated using DFT [6,7].

Therefore, in the present study we aim to employ the DFT + QTAIM to investigate the bonding properties and topologies of electron charge densities (TECDs) of two Zr-based Half-Heusler (HH) ZrXBi (X = Co, Rh) compounds. These materials have attracted increasing attentions because of their interesting thermoelectric properties [1,3,16–23]. We also intend to study the structural properties as well as electronic structures of these compounds including DOSs, band structures, and electron charge densities (ESDs) using DFT. Furthermore, we investigate the effects of imposing pressure on the TECDs and electronic structures of the

* Corresponding author.
E-mail address: sjalali@sci.ui.ac.ir (S. Jalali-Asadabadi).

https://doi.org/10.1016/j.jallcom.2020.154287
0925-8388/

compounds under question.

To validate our next new topological analysis, we first verify that the structural properties can be well predicted by GGA + U approach with our optimized U value for both of the cases in agreement with the available previous theoretical [3,23] and experimental [17,24] results. Our topological analysis demonstrates that the types and numbers of the critical points of ZrXBi (X = Co, Rh) are independent of the X atoms and our selected pressures imposed. However, bonds properties of these compounds depend on the X atoms and pressures imposed. As an important point, the bonds in ZrRhBi case are more stable than bonds in ZrCoBi case. Moreover, the charge values at bonds in the Rh-case are more than those in the Zr-case. For both the considered cases the stability of Zr-X (X = Co, Rh) bonds is increased by imposing pressure. Imposing pressure also increases the charge values at the bonds positions. Based on our calculations, the peak of total DOS of Co-case in the valence region is sharper and nearer to the Fermi level compared to the Rh-case. Band structure calculations reveal that both the compounds are semiconductors with indirect band gaps. The predicted band gap of Co-case is slightly more than that of the Rh-case. Moreover, a lower value is predicted for the hole effective masses in the Rh-case compared to the Co-case.

From our electronic properties analysis, it may be anticipated that the Seebeck coefficient of the Co-case is higher, while its electrical conductivity is lower than that of Rh-case. However, since these anticipations are made in the absence of the thermoelectric calculations, they can be trusted only when they are thermoelectrically verified, as well. Therefore, these anticipations are also quantitatively validated by calculating the Seebeck coefficient and electrical conductivity per relaxation time for both the compounds in question. This shows that our topological analysis presented in this work may be considered as a possible reliable foundation for further comprehensive thermoelectric study of these compounds.

2. Computational details

The structural properties and electronic structures of the compounds under question are calculated in the framework of the density functional theory (DFT) [6,7] using the full-potential augmented planewaves plus local orbitals (APW + lo) method [25,26], in the presence of the spin-orbit coupling (SOC), as embodied in the reliable WIEN2k code [27,28]. A mesh of 693 special *k*-points is considered in the irreducible wedge of the first Brillouin zone which corresponds to the grids of 17× 17× 17 in the Monkhorst-Pack scheme [29]. The Muffin-Tin radii (R_{MT}'s) are selected to be 2.4 for Zr, Rh, Co and 2.5 for Bi. The cutoff parameter of $K_{max} = 9.5/R_{MT}$ ($l_{max} = 10$) inside the Muffin-Tin spheres (interstitial region) is used for the expansions of the wavefunctions in terms of the lattice harmonics (planewaves). The periodic charge density and potential are Fourier expanded up to $G_{max} = 13$ Bohr^{-1}. In addition to the standard LDA and GGA functionals, we have used the GGA + U approach with several U values changing from 1 to 7 eV by step 1 eV.

The topological analysis of electron charge density (TECD) is carried out using the CRITIC2 code [30,31]. We have performed the topological calculations by a combination of DFT [6,7] and quantum theory of atoms in molecules (QTAIM) [8,9]. Topological analysis of electron charge density (ECD) distribution, $\rho(\mathbf{r})$, is done by determination of number, kind and position of its critical points (CPs). For each $\rho(\mathbf{r})$ distribution four kinds of CPs can be found; nuclear critical point (NCP or simply n), bond critical point (BCP or b), ring critical point (RCP or r) and cage critical point (CCP or c). More details of TECD calculations are presented in our recent work [5].

Thermoelectric parameters including Seebeck coefficient and electrical conductivity (σ) per relaxation time (τ), i.e., (σ/τ), are calculated using the BoltzTraP2 code [32] at T = 300 K. For these calculations a denser *k*-mesh including 3465 special *k*-points is considered in the irreducible wedge of the first Brillouin zone. More details of thermoelectric calculations (not represented here) including related formulas were previously presented [33–39] for other cases.

3. Structural properties

We have theoretically investigated the structural properties including lattice parameters (a) and bulk moduli (B_0) of ZrXBi compounds for X = Co and Rh. The structural properties are obtained by calculating the total energies of the unit cells as functions of their volumes and fitting the data with the Birch-Murnaghan isothermal equation of state [40]. We carried out these calculations employing LDA and GGA exchange-correlation functionals (XCFs) for 3 different configurations. The first one is configured to be non-magnetic (non-spin polarized). The two other configurations are magnetically ordered (spin polarized). The spin orientations in the second (third) configuration are ordered to be ↑↑↑ (↓↑↓) at Zr, X, and Bi atoms, respectively; *viz.* $Zr^{\uparrow}X^{\uparrow}Bi^{\uparrow}$ magnetic ordering for the second configuration and $Zr^{\downarrow}X^{\uparrow}Bi^{\downarrow}$ magnetic ordering for the third configuration, where X = Co, Rh. For convenient, we call the first (non-magnetic) configuration as Conf1, the second configuration as Conf2 and the third configuration as Conf3. According to our results, not only total magnetic moments of ZrXBi (X = Co, Rh) compounds but also their onsite magnetic moments at three Zr, X and Bi atoms are zero for these three different spin configurations, i.e. Conf1, Conf2, and Conf3, at the end of our well converged self-consistent calculations. In the other words, the calculated magnetic moments are found to be almost independent of the selected spin configurations in these ZrXBi (X = Co, Rh) compounds. The latter point, in turn, implies that these compounds most likely prefer to behave as non-magnetic systems, which is consistent with previous works [41–43,43]. Jiong Yang and coworkers [41], have counted the number of total valence electrons in the primitive half-Heusler (HH) unit cells of these compound and shown that each HH unit cell contains 18 electrons. Thus, based on the Slater-Pauling rule [42,43,43] the total magnetic moments of these systems are zero.

Table 1 shows the predicted lattice parameters and bulk moduli of the considered compounds using LDA and GGA XCFs along with the available previous theoretical and experimental results. In this table, the ground state energies of the compounds are also tabulated. As Table 1 reveals, our results are in good agreement with the previous results [3,23]. Our results show that Conf3 and Conf2 configurations lead to lower E_0 than Conf1 configuration. This is shown in Fig. 1 too. The magnetic moments of the compounds as obtained from the calculations are matching with the Slater Pauling's rule. However, the stable structure of the materials are not still clear from the calculations. Therefore, to clarify this we furthermore calculate the enthalpy for the systems using GGA XCF. The enthalpy is calculated by the $\Delta H = \Delta E + P\Delta V$ relation [44], where P is pressure, ΔV is volume, and ΔE is expressed by the following formula [44]:

$$\Delta E = E_{ZrXBi} - E_X - E_{Bi}, \quad (1)$$

where E_{ZrXBi} is the energy of ZrXBi (X = Co, Rh), E_X is the energy of X = Co, Rh, and E_{Bi} is the energy of Bi element. At zero pressure $\Delta H = \Delta E$. We calculate the enthalpies at zero pressure for the three spin configurations including NM (Conf1), FM (Conf2), and Ferri (Conf3). These calculations lead to the values of −0.08719 [-0.07822] and −0.08802 [-0.07893] eV as well as −0.08763 [-0.07836] eV for the enthalpies of the NM and FM as well as Ferri

Table 1
Lattice parameters (a) in Å, bulk moduli (B_0) in GPa and ground state energies (E_0) of ZrXBi (X = Co, Rh) in Ry using LDA and PBE-GGA approaches along with the other theoretical and experimental results. The results are presented for different spin configurations including non-magnetic, up spin directions for the three elements (↑ ↑ ↑) and dn up dn (↓ ↑ ↓) for Zr X and Bi, where X = Co, Rh. For simplicity, we label the first configuration as Conf1, the second configuration as Conf2 and the third configuration as Conf3.

ZrCoBi				
		a	B_0	E_0
Conf1	LDA	6.10	144.30	−53113.204763
	GGA	6.23	119.20	−53148.654121
Conf2	LDA	6.10	144.12	−53113.205633
	GGA	6.23	119.81	−53148.654966
		6.25[a]		
	HSE06[a]	6.15		
Conf3	LDA	6.10	144.45	−53113.205637
	GGA	6.23	120.1614	−53148.654968
Exp.[b]		6.18		
ZrRhBi				
		a	B_0	E_0
*Conf*1	LDA	6.32	146.64	−59892.385023
	GGA	6.45	123.34	−59932.321944
Conf2	LDA	6.32	147.51	−59892.387165
	GGA	6.45	122.23	−59932.322165
		6.44[c]	122.69[c]	
Conf3	LDA	6.32	147.52	−59892.387165
	GGA	6.45	122.19	−59932.322162
Exp.[d]		6.38		

[a] Reference [23].
[b] Reference [24].
[c] Reference [3].
[d] Reference [23].

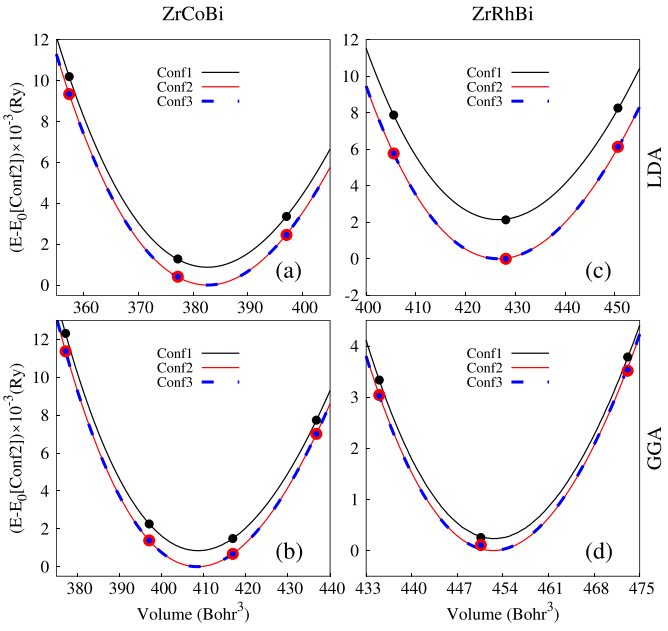

Fig. 1. Total energy of ZrXBi (X = Co, Rh) compounds versus volume calculated by (a) LDA for X = Co, (b) GGA for X = Co, (c) LDA for X = Rh, and (d) GGA for X = Rh in three different spin configurations; non-magnetic (Conf1), ferromagnetic (Conf2), and ferrimagnetic (Conf3). The energies are shown with respect to the ground state energy (E_0) of Conf2, i.e, E-E_0 [conf2].

phases of the Rh-case [Co-case], respectively. These results show that FM phase is a little bit more stable than the other phases.

The predicted bulk moduli are very slightly spin configuration dependent. However, the predicted lattice parameters are independent of spin configuration. These results are observed within both LDA and GGA XCFs. Based on our results, GGA predicts the lattice parameter of Co-case better than the LDA with respect to the experiment. For the Rh-case, the LDA result is slightly, i.e. 0.01, better than the GGA result compared to the experiment.

Although the GGA (LDA) leads to better results than the LDA (GGA) for ZrCoBi (ZrRhBi) with respect to the experiment, the lattice parameters predicted by LDA and GGA XCFs are far from the experiment. To improve the results, we have performed the calculations in Conf2 spin configuration within GGA + U as an another alternative approach. To obtain better result we have changed the U_{eff} parameter from 1 to 7 eV by step 1 eV. The results of these calculations are tabulated in Table 2 and shown in Fig. 2. As Table 2 reveals, the increase of U_{eff} parameter decreases the predicted lattice parameters of both the considered cases and makes them better compared to the experiment. Based on our result, the predicted lattice parameter for ZrCoBi by GGA + U with U_{eff} = 6 eV is in very good agreement with the experiment. Moreover, increase of U to 7 eV does not drastically change the result of U_{eff} = 6 eV. The result of GGA + U is comparable with the HSE06(24) result for ZrCoBi compound. Lattice parameter of ZrRhBi case is improved by increasing U_{eff} parameter too. However, the dependency of ZrRhBi lattice parameter to U_{eff} parameter is weaker than that of the ZrCoBi. According to the results presented in Tables 1 and 2, we can conclude that the GGA + U approach with U_{eff} = 6 eV is the most appropriate functional for the prediction of the structural properties of ZrXBi (X = Co, Rh) compounds among the considered functionals in the present work. The materials under study contain Zr, Rh and Co elements which their individual localization degrees can be different and system dependent. To verify the effects of the latter two points, we calculate the lattice parameter of ZrCoBi compound by considering a set of U-parameters which we apply on both Zr and Co simultaneously. The set of ($Ueff^{Co}$, $Ueff^{Zr}$) pari Hubbard U parameters for the (Co, Zr) pari elements is considered to be $\{(5,5), (5,6), (6,5), (6,6)\}$. In this set, the U_{eff} = 5 eV is

Table 2
Lattice parameters (a) in Å and bulk moduli (B_0) in GPa for ZrXBi (X = Co, Rh) using the GGA + U approach with U_{eff} = 1–7 eV employing the magnetic Conf2 spin configuration, i.e., up spin directions for the three elements (↑↑↑) along with the experimental results (25, 17). In GGA + U calculations the U parameter is considered for Co and Rh elements.

Comp		U_{eff}							Exp.
		1	2	3	4	5	6	7	
ZrCoBi	a	6.23	6.22	6.21	6.21	6.20	6.19	6.19	6.18[a]
	B_0	120.02	120.30	120.43	120.61	120.40	120.65	120.66	
ZrRhBi	a	6.44	6.44	6.43	6.43	6.43	6.42	6.42	6.38[b]
	B_0	122.30	123.26	123.26	123.51	123.08	122.73	122.70	

[a] Reference [24].
[b] Reference [17].

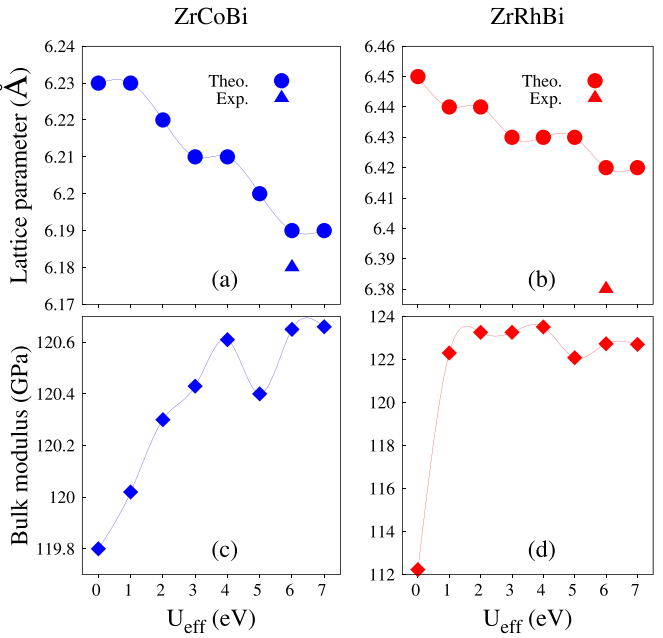

Fig. 2. Calculated lattice parameters in Å unit for (a) ZrCoBi and (b) ZrRhBi as well as bulk moduli (B_0) in GPa unit for (c) ZrCoBi and (d) ZrRhBi compounds using GGA + U versus U_{eff} along with the experimental results (Exp.) [17,24]. The results presented in this figure are obtained by including U_{eff} for Co in ZrCoBi and Rh in ZrRhBi.

considered, because it is the most suitable nearest value to the best value predicted by the results presented in Table 2, i.e., U_{eff} = 6 eV. We perform 4 individual lattice parameter calculations which in turn each of them include 7 self-consistent field (SCF) calculations and whence totally $7 \times 4 = 28$ SCF calculations by applying this set of U-values, as tabulated in Table 3. To perform two of these calculations, we first consider the U_{eff} = 5 eV for the Zr and then calculate the lattice parameter by considering individually U_{eff} = 5 eV and 6 eV for Co. For the next remaining two calculations we consider the U_{eff} = 6 eV for Zr and recalculate the lattice parameters by considering individually U_{eff} = 5 eV and 6 eV for Co. The results are tabulated in Table 3. The results, as tabulated in Tables 2 and 3, show that the lattice parameter of ZrCoBi compound increases and goes farther from (in worse agreement with) the experimental value by including the U parameter of Zr atom when U parameter of Co atom is also included. Similar results (not shown here) were obtained for the ZrRhBi compound. Thus, in this work we consider only the localization of X atom in ZrXBi compound by setting $Ueff^{Co}$ = 6 eV and report the results with this accuracy.

4. Electronic structure

In this section, we study the electronic structure of ZrXBi (X = Co, Rh) compounds, including the densities of states (DOSs), band structures and electron charge densities (ECDs) of the compounds employing GGA + U with U_{eff} = 6 eV XCF. As discussed in the previous section, the Conf3 leads to lower E_0 than the Conf1, while the Conf2 and Conf3 spin configurations lead to similar E_0 parameters for all of the considered cases. Moreover, the Conf2 leads to the lower enthalpy than Conf3. Thus, we performed the following calculations with Conf2 configuration. To investigate the effects of pressure on the electronic structures of the compounds, these calculations are reperformed also at P= 5 GPa pressure in addition to the calculations performed at zero pressure. The zero pressure is equivalent to $a = 6.19$ ($a = 6.42$) and 5 GPa is equivalent to a smaller lattice parameter of $a = 6.12$ ($a = 6.34$) for ZrCoBi (ZrRhBi), as calculated by the GGA + U with U_{eff} = 6 eV.

Table 3
Calculated lattice parameter of ZrCoBi compound in Å using GGA + U by considering U_{eff} = 5 and 6 eV for both Zr and Co, simultaneously along with the experimental data [24].

U–Zr	5		6	
U–Co	5	6	5	6
Theo	4.27	4.47	4.28	4.27
Exp. [24]	4.18			

4.1. Densities of states

Fig. 3 shows the DOSs of ZrXBi (X = Co, Rh) compounds calculated using GGA + U approach with U_{eff} = 6 eV at P= 0 and 5 GPa. The first row of this figure displays the total-DOSs and DOSs of the Zr-, X- and Bi-atoms of the compounds. The second (third) row displays the partial d-DOSs (d3/2- and d5/2-DOSs) of the Zr- and X-atoms. The first (third) column of Fig. 3 shows the DOSs of the Rh-case and the second (fourth) column shows the DOSs of the Co-case at zero (P= 5 GPa) pressure. The results at zero pressure show that the peaks of the total DOS and partial DOSs are piled up closer to the Fermi level and in narrower energy ranges for ZrCoBi case compared to those for ZrRhBi case, as would be observed by comparing the first and second columns of Fig. 3. Similar result can be seen at P= 5 GPa, see the third and fourth columns of Fig. 3. This my lead to higher Seebeck coefficient for Co-case than Rh-case [3,4]. The results at zero pressure also show that the valence bands of ZrXBi (X = Co, Rh) compounds are mainly dominated by the states of X-atoms, while the conduction bands are mostly consist of Zr-states, see Fig. 3 ($a_{1,j}$) for $j = 1, 2$. This result can be also seen at P= 5 GPa, see Fig. 3 ($b_{1,j}$) for $j = 1, 2$. Our calculations also reveal that the d-orbitals have the most contribution in the valence DOSs of X- and Zr-atoms at the two considered pressures, as shown in the second row of Fig. 3, i.e., Fig. 3 ($a_{2,j}$) and ($b_{2,j}$) for $j = 1, 2$. Both the valence spin up $d3/2$- and $d5/2$-DOSs of X-atoms have significantly contributed in both cases at both pressures,

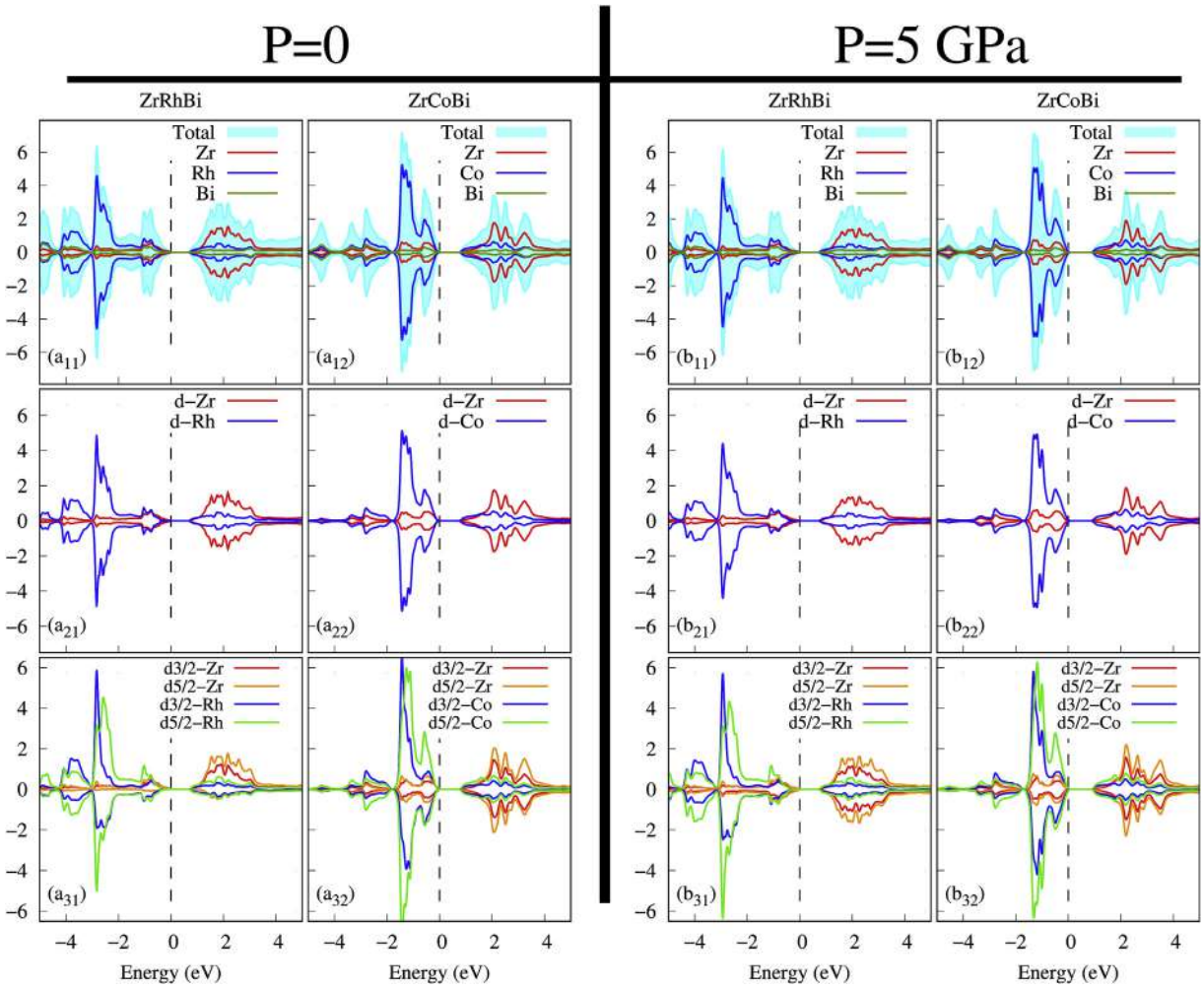

Fig. 3. Up and down densities of states of ZrXBi (X = Co, Rh) compounds at zero and P= 5 GPa pressures calculated by GGA + U approach with U_{eff} = 6 eV. The (a_{ij}) and (b_{ij}) labels of the figure refer to the zero and 5 GPa pressures, respectively, where $i = 1$ index, including the first row of the figure, refers to the total and atomic DOSs, and $i = 2$ ($i = 3$) index, including the second (third) row of the figure, refers to the partial d (d3/2 and d5/2) states of the Zr and X = Co, Rh elements. The $j = 1$ and 2 indexes, stand for the ZrRhBi and ZrCoBi compounds, respectively.

whereas the valence spin down $d5/2$-DOSs of the X-atoms have more significantly contributed than those of the $d3/2$-DOSs in both cases at both pressures, as shown in the third row, i.e., Fig. 3 ($a_{3,j}$) and ($b_{3,j}$) for $j = 1, 2$. The conduction spins up and down $d5/2$-DOSs of the Zr-atom have more significantly contributed than those of the $d3/2$-DOSs in both cases at both pressures, as shown in the third row, i.e., Fig. 3 ($a_{3,j}$) and ($b_{3,j}$) for $j = 1, 2$.

4.2. Band structure

Fig. 4 displays the spins up and down band structures of ZrXBi (X = Co, Rh) compounds at zero and 5 GPa pressures. In this figure, the d-Zr and d-X (X = Co, Rh) states are also characterized by the thickness of bands; the larger thickness of the bands, the more contribution of the d-states. These band structures are calculated by the GGA + U approach with U_{eff} = 6 eV. As shown in this figure, both compounds are semiconductors with indirect band gaps at both the considered pressures. In both cases, the valence band maximum (VBM) occurs at the Γ-symmetry point, while conduction band minimum (CBM) lies in the X-symmetry point. Moreover, the most contribution of the d-Zr (d-X) states are seen in the CBM (VBM). Based on Fig. 4, the bands of Co-case at/near the VBM are considerably flatter than those of Rh-case. This predicts higher values for the effective mass in ZrCoBi compared to that in ZrRhBi. This result is seen at both the considered pressures. The band gaps of the compounds calculated using the GGA + U approach with U_{eff} = 6 eV at zero and 5 GPa pressures, along with the results of other calculations [3,23] are tabulated in Table 4. According to the results presented in this table, the band gaps predicted by GGA + U are less than those predicted by GGA [3,23] for both cases at zero pressure. The HSE06 [23] predicts the band gap of Co-case more than the GGA and GGA + U at zero pressure. Comparing the band gaps calculated by GGA + U at the two pressures reveals that imposing pressure increases the band gaps of both compounds. As Table 4 indicates, the band gap of Rh-case is less than that of the Co-case at P = 0 as well as P= 5 GPa using GGA + U. Lower band gap of the Rh-case makes the thermal excitation of electrons more easier in this case than that in the Co-case, which may cause higher electrical conductivity in the Rh-case compared to the Co-case [3]. Based on our electronic structure analyses, one may predict that the Co-case has higher [lower] Seebeck coefficient [electrical conductivity] than Rh-case. However, these predictions can be only validated in the presence of thermoelectric results. Therefore, let us a little bit deviate from the main subject of this work which is topological analyses, and calculate the Seebeck coefficient and electrical conductivity (σ) per relaxation time (τ), i.e., (σ/τ), for the

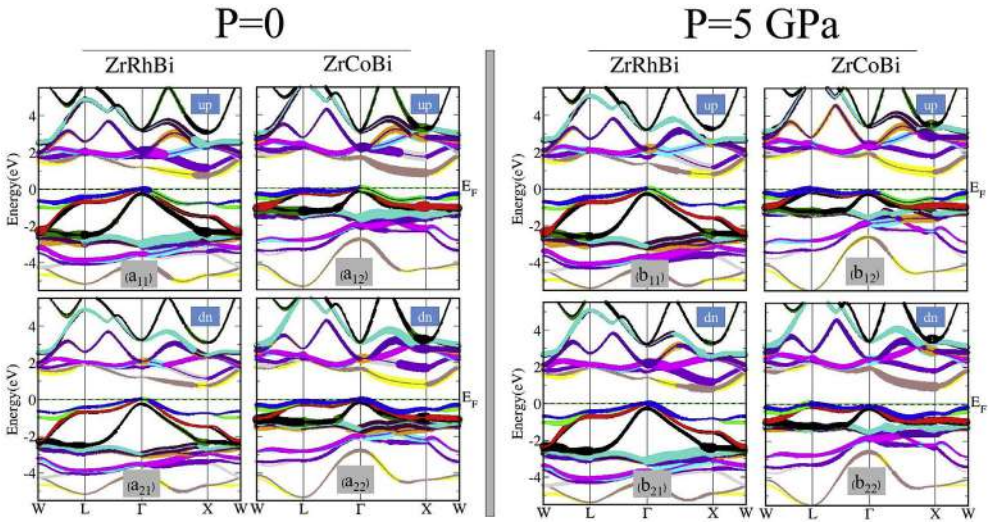

Fig. 4. Band structures of ZrXBi (X = Co, Rh) compounds for up and down spins at zero as well as P= 5 GPa pressures calculated by GGA + U approach with U_{eff} = 6 eV. The a and b labels refer to zero and 5 GPa pressures, respectively. The i = 1 and 2 indexes refer to up and down spin bands, respectively. The j = 1 (j = 2) index refers to the Rh (Co-case).

Table 4
Band gaps of ZrXBi (X = Co, Rh) compounds at P = 0 and P= 5 GPa pressures in eV unit. These gaps are calculated by GGA + U approach with U_{eff} = 6 eV.

Compound	XCF	P = 0	P= 5 GPa
ZrCoBi	GGA + U	0.822	0.956
	GGA[a]	1.01	
	HSE06[a]	1.34	
ZrRhBi	GGA + U	0.739	0.783
	GGA[b]	1.02	

[a] Reference [23].
[b] Reference [3].

ZrCoBi and ZrRhBi compounds using GGA + U with U_{eff} = 6 eV at T = 300 K. Our calculations lead to 96 $\frac{\mu V}{K}$ [81 $\frac{\mu V}{K}$] for the Seebeck coefficient, and $5.45\times10^{11}\frac{1}{\Omega.m.s}$ [$3.37\times10^{12}\frac{1}{\Omega.m.s}$] for the σ/τ of the Co-case [Rh-case]. These results show that the Seebeck coefficient of the Co-case is higher than that of the Rh-case, while the σ/τ of the Co-case is lower than that of the Rh-case, which are in agreement with our predictions made by the electronic calculations. Moreover, based on the electrical conductivity relation [32], lower σ/τ can be attributed to the higher electron effective mass. This agreements authenticate that there should be a relation between electronic structure and thermoelectric properties.

4.3. Electron charge density

Electron charge densities (ECDs) of the ZrXBi (X = Co, Rh) compounds in (001) and (01$\bar{1}$) planes are shown in Figs. 5 and 6, respectively. These ECDs are calculated using the GGA + U with U_{eff} = 6 eV at zero and P= 5 GPa pressures. The results presented in Fig. 5 (Fig. 6) show that the ECDs of both compounds do not behave very differently from each other in (001)-plane ((01$\bar{1}$)-plane) at both zero and 5 GP pressures. The main of ECDs, as shown in Figs. 5 and 6, are almost spherically distributed near the atomic positions in (001)- and (01$\bar{1}$)-planes. This result is consistent with the reported results for $CeMIn_5$ (M = Co, Rh) cases.(5) The ECDs are almost distributed uniformly outside the spheres-like charge distributions in (001)-plane for both compounds at both pressures, as shown in Fig. 5. In (01$\bar{1}$)-plane, however, the most of the ECDs, as distributed out of the spheres-like charge distributions, are accumulated in that direction of the (01$\bar{1}$)-plane where the X-atoms

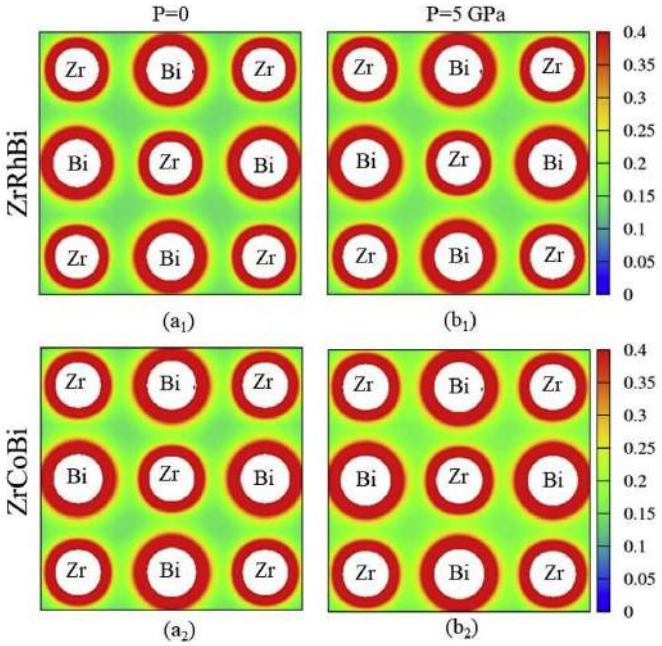

Fig. 5. Electron charge densities (ECDs) of ZrXBi (X = Co, Rh) compounds in (001)-plane at zero and 5 GPa pressures calculated by GGA + U with U_{eff} = 6 eV. The zero and 5 GPa pressures are labeled by (a_i) and (b_i), where i = 1 and i = 2 refer to the X = Rh and Co, respectively.

(X = Co, Rh) are located there, see Fig. 6. Fig. 6 shows a blue region in the left and right hand sides of the X (X = Co, Rh) atom on the (01$\bar{1}$)-plane. The blue color, as scaled in the right hand side of this figure, is equivalent to the least ECD or a minimum of the ECD distribution in (01$\bar{1}$)-plane. Each of the blue regions are surrounded by a thin yellow corona which is itself surrounded by another thin green corona on (01$\bar{1}$)-plane for both compounds at both pressures. In the right hand side of the X (X = Co, Rh) atom on the (01$\bar{1}$)-plane, a thin yellow line between the Zr-atoms and a green line between Zr- and Bi-atoms can be seen in (01$\bar{1}$)-plane for both compounds at both pressures. By keeping in mind the color scale and the positions of the atoms in the (01$\bar{1}$)-plane, as shown in Fig. 6, one observes

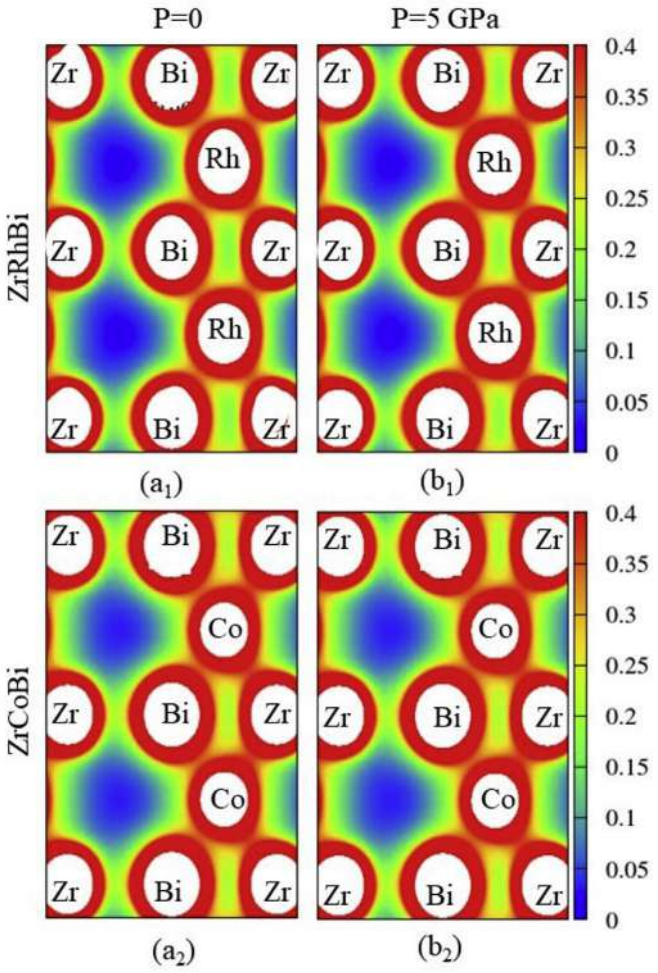

Fig. 6. Electron charge densities (ECDs) of ZrXBi (X = Co, Rh) compounds in $(01\bar{1})$-plane at zero and 5 GPa pressures calculated by GGA + U with U_{eff} = 6 eV. The zero and 5 GPa pressures are labeled by (a_i) and (b_i), where $i = 1$ and $i = 2$ refer to the X = Rh and Co, respectively.

that the two Zr atoms located in the right hand side of the X (X = Co, Rh) atom are weakly connected to each other, *viz.* the Zr–Zr right-hand-side-bonds are weak. Similarly, the Zr–Bi bonds are weak in the $(01\bar{1})$-plane. Therefore, there are minima of ECDs between the Zr and Bi atomic positions as well as between the Zr and Zr atomic positions. However, the ECD scaled by green color between Zr and Bi atoms is higher than the ECD scaled by blue color between the Zr-atoms. Thus, the minima of ECDs in the Zr–Bi bonds (with green color) are higher compared to the Zr–Zr bonds (with blue color). The red ECDs around the Zr and X atomic positions are connected to each other by orange color regions. Each of these orange regions are surrounded by a yellow corona. The ECD shown by orange color is scaled to be higher (lower) than that scaled by yellow (red) color. This can be considered as a surface that curves up in one direction, while it curves down in another different direction. In both of the directions, the derivatives become zero without showing a local extremum (minimum or maximum) on both directions, resembling a riding saddle critical point in the domain of the ECDs shown in Fig. 6. Saddle point can be defined as a stationary point of a two-variables function where the partial derivatives of its orthogonal components vanish without having a local maximum or minimum on both orthogonal axes. Thus, we expect a saddle point in the region with orange color. Similar result is seen between Bi and X (X = Co, Rh) atoms. The discussed ECD results are valid for both the compounds and pressures under study.

Table 5
Number and types of non-equivalent CPs for ZrXBi (X = Co, Rh), calculated by GGA + U functional with U_{eff} = 6 eV at P = 0 and 5 GPa pressures. The numbers in parentheses represent the number of equivalent CPs.

	Pressure (GPa)	NCP	BCP	RCP	CCP
ZrCoBi	0	3(12)	2(32)	2(24)	1(4)
	5	3(12)	2(32)	2(24)	1(4)
ZrRhBi	0	3(12)	2(32)	2(24)	1(4)
	5	3(12)	2(32)	2(24)	1(4)

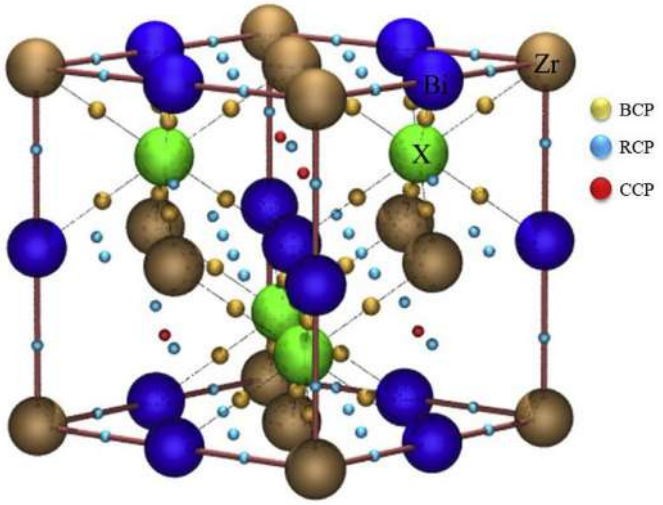

Fig. 7. Critical points (CPs) of ZrXBi (X = Co, Rh) compounds at zero pressure calculated using the GGA + U with U_{eff} = 6 eV.

5. Topological analysis

The CPs of ZrXBi (X = Co, Rh) compounds calculated by the GGA + U with U_{eff} = 6 eV are presented in Table 5 for P = 0 and 5 GPa pressures. The results show that the CP numbers of both the compounds satisfy the Morse condition, *viz*, $NCP - BCP + RCP - CCP = 0$, at the two considered pressures. Table 5 also shows that the numbers and types of CPs of both the compounds are the same as each other at P = 0 and P = 5 GPa. Comparing the numbers and types of CPs for ZrCoBi at zero and 5 GPa pressures indicate that imposing pressure does not change the numbers and types of CPs of this compound. Similar result can be seen for the other case, i.e., ZrRhBi.

The CPs of ZrXBi (X = Co, Rh) compounds at P = 0 are displayed in Fig. 7. Moreover, the numbers of CPs along with the flux lines generated by $\nabla\rho(\mathbf{r})$ (green curves), as well as $\nabla^2\rho(\mathbf{r})$ for both the compounds at zero and P= 5 GPa pressures are shown for the (001)-plane in Fig. 8 and for the $(01\bar{1})$-plane in Fig. 9. The results, as shown in Fig. 8, reveals that the numbers and types of CPs in (001)-plane of ZrXBi compounds do not depend on the X-atom and our considered pressures. Similar result, as shown in Fig. 9, can be seen in the $(01\bar{1})$-plane. According to the results presented in Fig. 8, there are not any bonds between the atoms in (001)-planes of the considered compounds at P = 0 and 5 GPa pressures. Instead, as shown in Fig. 8, there are RCPs on the lines connecting Zr atoms to each other and on the lines connecting Zr to Bi atoms in the (001)-plane of ZrXBi (X = Co, Rh) at both the considered pressures. The BCPs can be seen, however, in the $(01\bar{1})$-planes, see Fig. 9. These BCPs are there between the Bi and X, as labeled by b1, and between

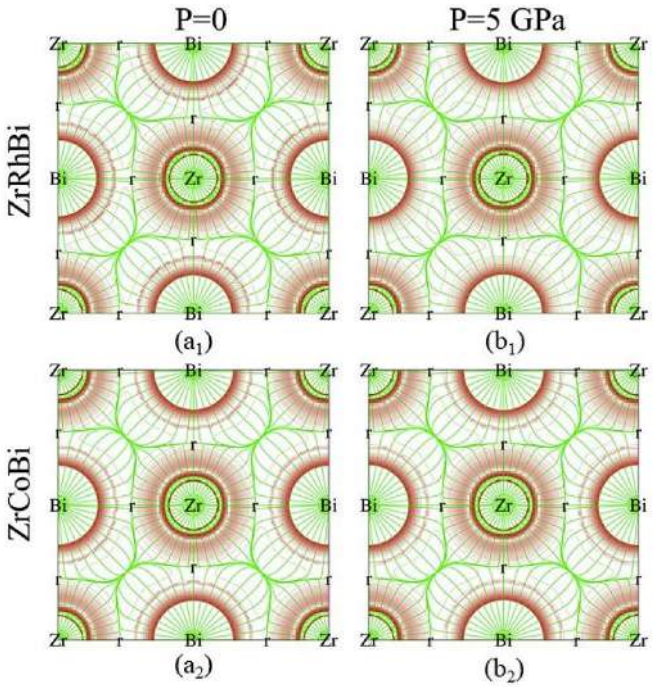

Fig. 8. CPs (c, b, r characters), and flux lines generated by $\nabla\rho(\mathbf{r})$ (green curves), as well as $\nabla^2\rho(\mathbf{r})$ (red curves) in the (001)-plane of ZrXBi (X = Co, Rh) compounds at zero and 5 GPa pressures calculated using the GGA + U with U_{eff} = 6 eV. The (a_i) [(b_i)] labels with $i = 1, 2$ refer to the zero [5 GPa] pressure, while the $i = 1[i = 2]$ index refers to the X = Rh [X = Co]. (For interpretation of the references to color in this figure legend, the reader is referred to the Web version of this article.)

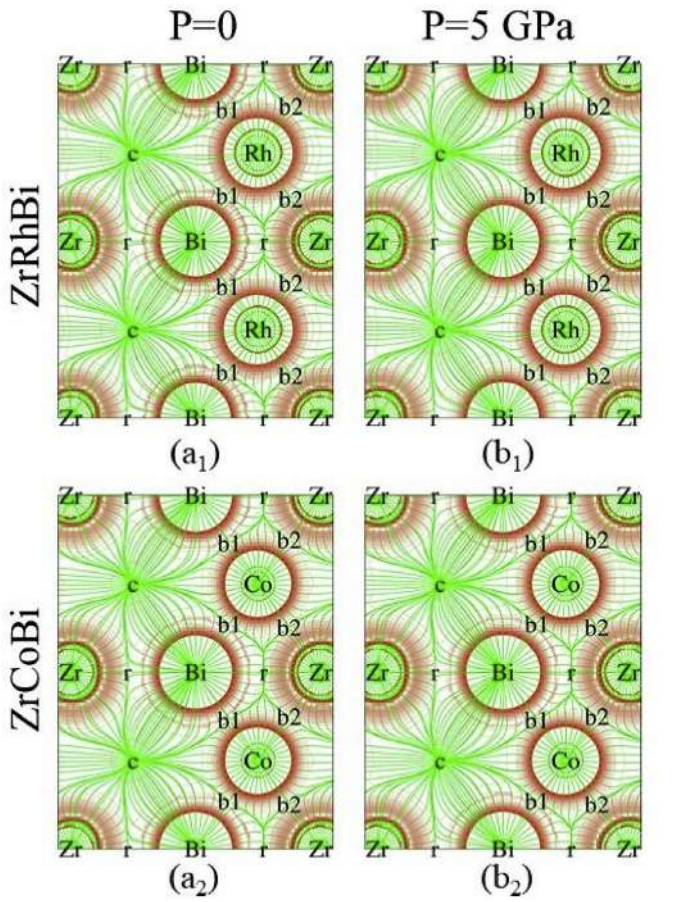

Fig. 9. CPs (c, b, r characters), and flux lines generated by $\nabla\rho(\mathbf{r})$ (green curves), as well as $\nabla^2\rho(\mathbf{r})$ (red curves) in the $(01\bar{1})$-plane of ZrXBi (X = Co, Rh) compounds at zero and 5 GPa pressures calculated using the GGA + U with U_{eff} = 6 eV. The (a_i) [(b_i)] labels with $i = 1, 2$ refer to the zero [5 GPa] pressure, while the $i = 1[i = 2]$ index refers to the X = Rh [X = Co]. (For interpretation of the references to color in this figure legend, the reader is referred to the Web version of this article.)

the Zr- and X-atoms, as labeled by b2, where X = Co, Rh. As can be seen from the data presented in Table 5, the ZrXBi compound has one non-equivalent CCP for X = Co, Rh. This CCP is located on the $(01\bar{1})$-plane for both the compounds at both the pressures, as shown in Fig. 9. The results, as presented in Fig. 9, show that there are not any CPs on the lines connecting the Zr atoms in $(01\bar{1})$-planes of the compounds at both the considered pressures.

As discussed in Sec. 1, bond properties can affect the thermoelectric properties of materials. Therefore, the BCP properties of ZrCoBi and ZrRhBi cases are discussed below in more details. The BCPs and their properties are tabulated in Table 6 for ZrCoBi and ZrRhBi at zero and 5 GPa pressures. In this table, MULT is the multiplicity of the BCPs in the unit cell, d1 is the distance between BCP and ATOM1, d2 is the distance between BCP and ATOM2, $d1 - \widehat{b} - d2$ is the angle between ATOM1, BCP, and ATOM2 in degree, ρ, and $\nabla^2\rho$ are the values of ECD and its Laplacian evaluated at BCPs, respectively. Based on the data tabulated this table, ZrCoBi and ZrRhBi have some different BCP properties. The ρ and $\nabla^2\rho$ values of BCPs between Bi and X atoms, i.e. b1, and BCPs between Zr and X atoms, i.e. b2, in Co-case are less than those in the Rh-case at zero and 5 GPa pressures. Moreover, the ρ value at b1 is slightly more than that at b2 for X = Co at zero and 5 GPa pressures, while this trend is reversed for X = Rh. Furthermore, b2 is closer to (farther from) X than Zr when X = Co (X = Rh) at both the considered pressures. According to Table 6, imposing pressure increases the ρ and $\nabla^2\rho$ of BCPs for both of the Co- and Rh-cases. Although the $d1$ and $d2$ are changed by pressure, the $\frac{d1}{d2}$ fraction of BCPs is not drastically changed by imposing pressure. The $d1 - \widehat{b} - d2$ degrees are not also strongly related to the pressures or X atoms, for X = Co, Rh; the $d1 - \widehat{b} - d2$ degrees are very close to 180° for both cases at zero as well as 5 GPa pressure.

A large value of ρ and a large negative value of $\nabla^2\rho$ at a BCP may provide a covalent bond [45,46]. In contrast, a small value of ρ and a large positive value of $\nabla^2\rho$ at a BCP may provide an ionic bond [45,46]. However, our results show small values for both of the ρ and positive $\nabla^2\rho$ at all the BCPs of the considered cases. This can be taken as an indication to the fact that the ZrXBi (X = Co, Rh) may not be considered as purely ionic or purely covalent compounds. Instead, they may be composed of a mixture of ionic and covalent bonds such as LiH and NaH compounds as previously reported by Lixian Zhang and coworkers [45]. Although the ρ and $\nabla^2\rho$ of BCPs are increased by imposing pressure, this latter result remains valid at P= 5 GPa, as well.

Stability of a bond can be quantified by the directionality which can be defined by two components: [15,47]

$$\tan\alpha = \sqrt{\frac{\lambda_\perp}{\lambda_\parallel}}, \quad \tan\beta = \sqrt{\frac{\lambda'_\perp}{\lambda_\parallel}}, \tag{2}$$

where α and β angles represent the extreme angles of the elliptic cone constructed by the Hessian of charge density at the BCP and surrounding the bond path. The $\lambda_\parallel$ is the positive eigenvalue of ECD Hessian matrix at the given BCP and represents the principal curvature along the bond path. The $\lambda_\perp$ and $\lambda'_\perp$ ($|\lambda_\perp| \geq |\lambda'_\perp|$) are two negative eigenvalues of ECD Hessian matrix at the given BCP and represent the principal curvatures perpendicular to the bond path.

Table 6
BCPs and their properties, including MULT as multiplicity of the BCPs in the unit cell; d1 as the distance between BCP and ATOM1; d2 as the distance between BCP and ATOM2; d1 − $\widehat{b}$ − d2 as the angle between ATOM1, BCP, and ATOM2 in degree; ρ, and $\nabla^2\rho$ as the values of ECD and its Laplacian evaluated at BCPs for ZrCoBi and ZrRhBi at zero and 5 GPa by GGA + U functional with U_{eff} = 6 eV.

	P = 0									
	BCP	MULT	ATOM1	ATOM2	d1 (bohr)	d2 (bohr)	$\frac{d1}{d2}$	d1 − $\widehat{b}$ − d2	$\rho\left(\frac{elec}{bohr^3}\times 110^{-2}\right)$	$\nabla^2\rho\left(\frac{elec}{bohr^5}\times 110^{-2}\right)$
ZrCoBi	b1	16	Co	Bi	2.3199	2.7499	0.8436	179.9985	4.8621	6.8265
	b2	16	Co	Zr	2.5144	2.5554	0.9839	179.9987	4.8247	3.2287
ZrRhBi	b1	16	Rh	Bi	2.5484	2.7074	0.9413	179.9999	4.8824	7.9546
	b2	16	Rh	Zr	2.7533	2.5026	1.1002	179.9961	4.9726	4.8325
	P= 5 GPa									
	BCP	MULT	ATOM1	ATOM2	d1 (bohr)	d2 (bohr)	$\frac{d1}{d2}$	d1 − $\widehat{b}$ − d2	$\rho\left(\frac{elec}{bohr^3}\times 110^{-2}\right)$	$\nabla^2\rho\left(\frac{elec}{bohr^5}\times 110^{-2}\right)$
ZrCoBi	b1	16	Co	Bi	2.2927	2.7130	0.8451	179.9984	5.1430	7.3602
	b2	16	Co	Zr	2.4838	2.5219	0.9849	179.9990	5.0946	4.2092
ZrRhBi	b1	16	Rh	Bi	2.5109	2.6800	0.9369	179.9999	5.4094	8.7162
	b2	16	Rh	Zr	2.7197	2.4712	1.1006	179.9964	5.3793	5.5002

Table 7
Directionality represented by tanα and tanβ accompanied by ellipticity ε of bonds of ZrXBi (X = Co, Rh) compounds at zero pressure as well as 5 GPa calculated within GGA + U functional with U_{eff} = 6 eV.

	ZrCoBi				ZrRhBi			
P (GPa)	BCP	tanα	tanβ	ε	BCP	tanα	tanβ	ε
0	b1	0.42	0.42	0.00	b1	0.43	0.43	0.00
	b2	0.58	0.58	0.00	b2	0.55	0.55	0.00
5	b1	0.42	0.42	0.00	b1	0.43	0.43	0.00
	b2	0.56	0.56	0.00	b2	0.54	0.54	0.00

Larger values of directionality means that the bond is further from the topological instability. The directionality of bonds of ZrXBi (X = Co, Rh) compounds are tabulated in Table 7. From the data presented in this table, one observes that the tanα and tanβ of the b1 BCP in ZrRhBi case are slightly more than those in ZrCoBi case at both the considered pressures. Similar trend can be seen for the b2 BCP. Thus, it can be concluded that the BCPs in Rh-case are slightly more stable compared to the Co-case. Comparing the tanα and tanβ of b1 (b2) BCPs in Co-case at zero and 5 GPa pressures shows that imposing this pressure does not change (increases) the stability of b1 (b2) bond. The same result is seen for the ZrRhBi case.

In Table 7, ellipticity (ε) of BCPs are also represented. The ellipticity of a bond provides a measure of the extent to which charge is accumulated in the plane constructed by the eigenvectors with negative eigenvalues and is defined as [9]:

$$\varepsilon = \frac{|\lambda_\perp|}{|\lambda'_\perp|} - 1; \qquad |\lambda_\perp| > |\lambda'_\perp|, \tag{3}$$

Bonds with $\varepsilon = 0$ have cylindrical symmetry. Thus, this quantity shows the deviation from the cylindrical symmetry. As presented in Table 7, the ε parameter is zero for all of the BCPs in Co- and Rh-case at zero and 5 GPa pressures. This shows that BCPs of these cases have cylindrical symmetry.

6. Conclusion

In this work, we have investigated the structural and electronic properties, including densities of states (DOSs), band structures, and electron charge densities (ECDs), as well as topology of ECDs (TECDs) of two half-Heusler ZrCoBi and ZrRhBi compounds using a combination of the density functional theory (DFT) and quantum theory of atoms in molecules (QTAIM). Thermoelectric parameters of these compounds, including Seebeck coefficient and electrical conductivity are also calculated at zero pressure and room temperature. Structural properties calculations are carried out in different magnetic phases, including non-magnetic (NM), ferromagnetic (FM) and ferrimagnetic (Ferri). Based on the results, FM and Ferri phases are more stable than NM phase. Even though FM and Ferri have approximately the same ground state energy, our enthalpy calculations at zero pressure show more stability for the FM phase than the Ferri phase. Based on our calculations, GGA + U approach with U_{eff} = 6 eV predicts the structural properties of the compounds under study in agreement with the experimental data. The electronic structural calculations indicate the DOS of Co-case has a sharp peak near the Fermi level, while for the Rh-case the peak of DOS is further from the Fermi level and broader than that for the Co-case. Our band structure calculations show smaller band gap for the Rh-case than Co-case. These calculations also reveal higher effective mass of the carriers in ZrCoBi than ZrRhBi. Our electronic structure results predict higher electrical conductivity and lower Seebeck coefficient for the ZrRhBi compared to the ZrCoBi. These predictions are validated by our thermoelectric calculations. Our calculations show that imposing pressure slightly increases the band gaps of systems under study, but does not change the shapes of the bands and DOSs drastically. According to the TECD calculations, the cases under study have similar numbers and types of critical points (CPs). For both cases, only the bond critical points (BCPs) are seen between the Zr-X and Bi-X (X = Co, Rh) atomic positions, while between Zr−Zr and Zr−Bi atoms the ring critical points (RCPs) are observed. Although both cases have similar numbers and types of CPs, they have different BCP properties. The BCPs of Rh-case are more stable than those of the Co-case. Moreover, there are more charge value (ρ) at BCP positions of the Rh-case than Co-case. All of the BCPs in both cases have cylindrical symmetry at both the considered pressures. Based on the TECD results, the numbers and types of the CPs are not changed by imposing pressure, however, the ρ value and its Laplacian ($\nabla^2\rho$) are increased by imposing pressure. Moreover, the stability of BCPs between Zr and X atomic positions are slightly decreased by imposing pressure for both of the compounds. The results presented in this work may be used for further studies to improve the thermoelectric efficiencies of these materials.

Declaration of competing interest

The authors declare that they have no known competing

financial interests or personal relationships that could have appeared to influence the work reported in this paper.

CRediT authorship contribution statement

M. Yazdani-Kachoei: Conceptualization, Data curation, Formal analysis, Investigation, Methodology, Validation, Visualization, Writing - original draft. **S. Jalali-Asadabadi:** Conceptualization, Data curation, Formal analysis, Funding acquisition, Investigation, Methodology, Project administration, Resources, Software, Supervision, Validation, Visualization, Writing - review & editing.

Acknowledgements

This work, as a aprt of postdoctoral propject of Majid Yazdani-Kachoei, is supported by the University of Isfahan (UI).

References

[1] H. Zhu, R. He, J. Mao, Q. Zhu, C. Li, J. Sun, W. Ren, Y. Wang, Z. Liu, Z. Tang, A. Sotnikov, Z. Wang, D. Broido, D.J. Singh, G. Chen, K. Nielsch, Z. Ren, Discovery of zrcobi based half heuslers with high thermoelectric conversion efficiency, Nat. Commun. 9 (1) (2018) 2497.

[2] E.S. Toberer, L.L. Baranowski, C. Dames, Advances in thermal conductivity, Annu. Rev. Mater. Res. 42 (1) (2012) 179–209, https://doi.org/10.1146/annurev-matsci-070511-155040, arXiv:.

[3] J. Vikram, Enamullah Kangsabanik, A. Alam, Bismuth based half-heusler alloys with giant thermoelectric figures of merit, J. Mater. Chem. A 5 (2017) 6131–6139, https://doi.org/10.1039/C7TA00920H.

[4] G.D. Mahan, J.O. Sofo, The best thermoelectric, Proc. Natl. Acad. Sci. Unit. States Am. 93 (15) (1996) 7436–7439, https://doi.org/10.1073/pnas.93.15.7436, arXiv:https://www.pnas.org/content/93/15/7436.full.pdf, https://www.pnas.org/content/93/15/7436.

[5] M. Yazdani-Kachoei, S. Jalali-Asadabadi, N. Arianmehr, Topological analysis of $cemin_5$ (m = Co, Rh) electron charge densities, Comput. Mater. Sci. 164 (2019) 205–217, https://doi.org/10.1016/j.commatsci.2019.03.041. http://www.sciencedirect.com/science/article/pii/S0927025619301776.

[6] P. Hohenberg, W. Kohn, Inhomogeneous electron gas, Phys. Rev. 136 (1964) B864–B871. http://link.aps.org/doi/10.1103/PhysRev.136.B864.

[7] W. Kohn, L.J. Sham, Self-consistent equations including exchange and correlation effects, Phys. Rev. 140 (1965) A1133–A1138. http://link.aps.org/doi/10.1103/PhysRev.140.A1133.

[8] R.F.W. Bader, A quantum theory of molecular structure and its applications, Chem. Rev. 91 (5) (1991) 893–928, https://doi.org/10.1021/cr00005a013.

[9] R.F.W. Bader, Atoms in Molecules: A Quantum Theory (International Series of Monographs on Chemistry), Oxford University Press, 1994.

[10] T. Stürzer, G. Derondeau, D. Johrendt, Role of different negatively charged layers in $Ca_{10}(FeAs)_{10}(Pt_4As_8)$ and superconductivity at 30 k in electron-doped $(Ca_{0.8}La_{0.2})_{10}(FeAs)_{10}(Pt_3As_8)$, Phys. Rev. B 86 (2012) 60516, https://doi.org/10.1103/PhysRevB.86.060516.

[11] M.E. Eberhart, T.E. Jones, Cauchy pressure and the generalized bonding model for nonmagnetic bcc transition metals, Phys. Rev. B 86 (2012) 134106, https://doi.org/10.1103/PhysRevB.86.134106.

[12] A. Forni, D. Franchini, F. Dapiaggi, S. Pieraccini, M. Sironi, P. Scilabra, T. Pilati, K.I. Petko, G. Resnati, Y.L. Yagupolkii, Featuring in halogen bond and weaker interactions in iodoperfluoroalkylimidazoles: an experimental and theoretical charge density study, Cryst. Growth Des. 19 (3) (2019) 1621–1631, https://doi.org/10.1021/acs.cgd.8b01483, arXiv:.

[13] G. Saleh, A.R. Oganov, Alkali subhalides: high-pressure stability and interplay between metallic and ionic bonds, Phys. Chem. Chem. Phys. 18 (2016) 2840–2849, https://doi.org/10.1039/C5CP06026E.

[14] T.E. Jones, M.E. Eberhart, D.P. Clougherty, Topology of the spin-polarized charge density in bcc and fcc iron, Phys. Rev. Lett. 100 (2008) 17208, https://doi.org/10.1103/PhysRevLett.100.017208.

[15] T.E. Jones, M.E. Eberhart, D.P. Clougherty, Topology of the spin-polarized charge density in bcc and fcc iron, Phys. Rev. Lett. 100 (2008), 017208.

[16] J. Zhou, H. Zhu, T.-H. Liu, Q. Song, R. He, J. Mao, Z. Liu, W. Ren, B. Liao, D.J. Singh, Z. Ren, G. Chen, Large thermoelectric power factor from crystal symmetry-protected non-bonding orbital in half-heuslers, Nat. Commun. 9 (1) (2018) 1721.

[17] R. Gautier, X. Zhang, L. Hu, L. Yu, Y. Lin, T. O. L. Sunde, D. Chon, K. R. Poeppelmeier, A. Zunger, Prediction and accelerated laboratory discovery of previously unknown 18-electron abx compounds, Nat. Chem..

[18] M. Zahedifar, P. Kratzer, Band structure and thermoelectric properties of half-heusler semiconductors from many-body perturbation theory, Phys. Rev. B 97 (2018) 35204, https://doi.org/10.1103/PhysRevB.97.035204. https://link.aps.org/doi/10.1103/PhysRevB.97.035204.

[19] F. Chenguang, B. Shengqiang, Y. Liu1, T. Yunshan, C. Lidong, Z. Xinbing, Z. Tiejun, Realizing high figure of merit in heavy-band p-type half-heusler thermoelectric materials, Nat. Commun..

[20] H. Xie, H. Wang, C. Fu, et al., The intrinsic disorder related alloy scattering in ZrNiSn half-Heusler thermoelectric materials, Sci. Rep. 4 (2015) 6888.

[21] F. Casper, T. Graf, S. Chadov, B. Balke, C. Felser, Half-heusler compounds: novel materials for energy and spintronic applications, Semicond. Sci. Technol. 27 (6) (2012) 63001, https://doi.org/10.1088/0268-1242/27/6/063001.

[22] A.J. Hong, L. Li, R. He, J.J. Gong, Z.B. Yan, K.F. Wang, J.M. Liu, Z.F. Ren, report Full-scale Computation for All the Thermoelectric Property Parameters of Half-Heusler Compounds, Sci. Rep. 6 (2016) 22778.

[23] G. Fiedler, P. Kratzer, Ternary semiconductors nizrsn and cozrbi with half-heusler structure: a first-principles study, Phys. Rev. B 94 (2016) 75203, https://doi.org/10.1103/PhysRevB.94.075203. https://link.aps.org/doi/10.1103/PhysRevB.94.075203.

[24] C.B. Evers, C.G. Richter, K. Hartjes, W. Jeitschko, Ternary transition metal antimonides and bismuthides with mgagas-type and filled nias-type structure1dedicated to professor riccardo ferro on the occasion of his 70th birthday.1, J. Alloys Compd. 252 (1) (1997) 93–97, https://doi.org/10.1016/S0925-8388(96)02616-3. http://www.sciencedirect.com/science/article/pii/S0925838896026163.

[25] E. Sjöstedt, L. Nordström, D. Singh, An alternative way of linearizing the augmented plane-wave method, Solid State Commun. 114 (1) (2000) 15–20. http://www.sciencedirect.com/science/article/pii/S0038109899005773.

[26] G.K.H. Madsen, P. Blaha, K. Schwarz, E. Sjöstedt, L. Nordström, Efficient linearization of the augmented plane-wave method, Phys. Rev. B 64 (2001) 195134. http://link.aps.org/doi/10.1103/PhysRevB.64.195134.

[27] P. Blaha, K. Schwarz, G.K.H. Madsen, D. Kvasnicka, J. Luitz, R. Laskowski, F. Tran, L.D. Karks, WIEN2k, An Augmented Plane Wave + Local Orbitals Program for Calculating Crystal Properties, (Karlheinz Schwarz, Technische Universitat Wien), Vienna, Austria, 2018. ISBN 3-9501031-1-2.

[28] Blaha P., Schwarz K., Tran F., Laskowski R., Madsen G.K.H., Marks, L.D., WIEN2k: An APW+lo program for calculating the properties of solids, J. Chem. Phys. 152, (2020) 074101, doi: 10.1063/1.5143061.

[29] H.J. Monkhorst, J.D. Pack, Special points for brillouin-zone integrations, Phys. Rev. B 13 (1976) 5188–5192. http://link.aps.org/doi/10.1103/PhysRevB.13.5188.

[30] A.O. de-la Roza, E.R. Johnson, V. Luaña, Critic2: a program for real-space analysis of quantum chemical interactions in solids, Comput. Phys. Commun. 185 (3) (2014) 1007–1018.

[31] A.O. de-la Roza, M. Blanco, A.M. Pendás, V. Luaña, Critic: a new program for the topological analysis of solid-state electron densities, Comput. Phys. Commun. 180 (1) (2009) 157–166.

[32] G.K. Madsen, Jesús Carrete, M.J. Verstraete, Boltztrap2, a program for interpolating band structures and calculating semi-classical transport coefficients, Comput. Phys. Commun. 231 (2018) 140–145. http://www.sciencedirect.com/science/article/pii/S0010465518301632.

[33] M. Yazdani-Kachoei, S. Jalali-Asadabadi, Thermoelectric properties of heavy fermion cerhin5 using density functional theory combined with semiclassical Boltzmann theory, RSC Adv. 9 (2019) 36182–36197, https://doi.org/10.1039/C9RA07859B.

[34] M. Bilal, B. Khan, H.R. Aliabad, M. Maqbool, S.J. Asadabadi, I. Ahmad, Thermoelectric properties of sbnca3 and binca3 for thermoelectric devices and alternative energy applications, Comput. Phys. Commun. 185 (5) (2014) 1394–1398, https://doi.org/10.1016/j.cpc.2014.02.001. http://www.sciencedirect.com/science/article/pii/S0010465514000332.

[35] B. Khan, M. Yazdani-Kachoei, H.R. Aliabad, I. Khan, S. Jalali-Asadabadi, I. Ahmad, Effects of chemical potential on the thermoelectric performance of alkaline-earth based skutterudites (afe4sb12, aca, sr and ba), J. Alloys Compd. 694 (2017) 253–260, https://doi.org/10.1016/j.jallcom.2016.09.308. http://www.sciencedirect.com/science/article/pii/S0925838816330717.

[36] H.R. Aliabad, Z. Barzanuni, S.R. Sani, I. Ahmad, S. Jalali-Asadabadi, H. Vaezi, M. Dastras, Thermoelectric and phononic properties of (gd, tb) mno3 compounds: Dft calculations, J. Alloys Compd. 690 (2017) 942–952, https://doi.org/10.1016/j.jallcom.2016.08.167. http://www.sciencedirect.com/science/article/pii/S0925838816325464.

[37] M. Bilal, Saifullah, M. Shafiq, B. Khan, H.R. Aliabad, S.J. Asadabadi, R. Ahmad, I. Ahmad, Antiperovskite compounds sbnsr3 and binsr3: potential candidates for thermoelectric renewable energy generators, Phys. Lett. 379 (3) (2015) 206–210, https://doi.org/10.1016/j.physleta.2014.11.016. http://www.sciencedirect.com/science/article/pii/S037596011401144X.

[38] mB. Khan, H.R. Aliabad, N. Razghandi, M. Maqbool, S.J. Asadabadi, I. Ahmad, Structural and thermoelectric properties of pure and la, y doped homno3 for their use as alternative energy materials, Comput. Phys. Commun. 187 (2015) 1–7, https://doi.org/10.1016/j.cpc.2014.09.015. http://www.sciencedirect.com/science/article/pii/S001046551400321X.

[39] R. Iqbal, M. Bilal, S. Jalali-Asadabadi, H.A. Rahnamaye Aliabad, I. Ahmad, Theoretical investigation of thermoelectric and elastic properties of intermetallic compounds sctm (tm = cu, ag, au and pd), 02, Int. J. Mod. Phys. B 32 (2018) 1850004, https://doi.org/10.1142/S0217979218500042. arXiv:.

[40] F. Birch, Finite elastic strain of cubic crystals, Phys. Rev. 71 (1947) 809–824, https://doi.org/10.1103/PhysRev.71.809.

[41] J. Yang, H. Li, T. Wu, W. Zhang, L. Chen, J. Yang, Evaluation of half-heusler compounds as thermoelectric materials based on the calculated electrical transport properties, Adv. Funct. Mater. 18 (19) (2008) 2880–2888, https://doi.org/10.1002/adfm.200701369, arXiv: https://onlinelibrary.wiley.com/doi/pdf/10.1002/adfm.200701369 https://onlinelibrary.wiley.com/doi/abs/10.

1002/adfm.200701369.
[42] J. Ma, V.I. Hegde, K. Munira, Y. Xie, S. Keshavarz, D.T. Mildebrath, C. Wolverton, A.W. Ghosh, W.H. Butler, Computational investigation of half-heusler compounds for spintronics applications, Phys. Rev. B 95 (2017) 24411, https://doi.org/10.1103/PhysRevB.95.024411. https://link.aps.org/doi/10.1103/PhysRevB.95.024411.
[43] I. Galanakis, P.H. Dederichs, N. Papanikolaou, Origin and properties of the gap in the half-ferromagnetic heusler alloys, Phys. Rev. B 66 (2002) 134428, https://doi.org/10.1103/PhysRevB.66.134428. https://link.aps.org/doi/10.1103/PhysRevB.66.134428.
[44] P.A. Korzhavyi, A.V. Ruban, A.Y. Lozovoi, Y.K. Vekilov, I.A. Abrikosov, B. Johansson, Constitutional and thermal point defects in *b2* nial, Phys. Rev. B 61 (2000) 6003–6018, https://doi.org/10.1103/PhysRevB.61.6003. https://link.aps.org/doi/10.1103/PhysRevB.61.6003.
[45] L. Zhang, F. Ying, W. Wu, P. Hiberty, S. Shaik, Topology of electron charge density for chemical bonds from valence bond theory: a probe of bonding types, Chem. Eur J. 15 (12) (2009) 2979–2989, https://doi.org/10.1002/chem.200802134.
[46] S. Fahad, G. Murtaza, T. Ouahrani, R. Khenata, M. Yousaf, S. Omran, S. Mohammad, Structural, elastic, electronic, bonding, and optical properties of $BeAZ_2$ (A = Si, Ge, Sn; Z = P, As) chalcopyrites, J. Alloys Compd. 646 (2015) 211–222. http://www.sciencedirect.com/science/article/pii/S0925838815301444.
[47] M. Eberhart, From topology to geometry, Can. J. Chem. 74 (6) (1996) 1229–1235.